CrystEngComm

Accepted Manuscript

ROYAL SOCIETY OF CHEMISTRY

www.rsc.org/crystengcomm

ARTICLE TYPE www. rsc.org/xxxxxx | XXXXXXXX

Tuning the magnetic properties of FeCo with pulsed DC magnetron sputtering

M. Abuín,*[a,b] L. Pérez,[b,c] A. Mascaraque[b,c] and M. Maicas,[d]

Received Xth XXXXXXXXXX 20XX, Accepted Xth XXXXXXXXX 20XX
First published on the web Xth XXXXXXXXXX 200X
DOI: 10.1039/b000000x

We report a comparison of the magnetic properties of $Fe_{53}Co_{47}$ grown with DC and Pulsed DC (PDC) sputtering sources. While no remarkable differences concerning structure and composition are found, films grown by PDC reduce their coercivity in several times that in samples grown by DC sources under similar conditions. In addition, PDC films exhibit hard axis rocking effects and a better defined anisotropy axis. By means of EXAFS we have measured the atomic distances of the FeCo matrix and bcc-Co clusters. We show that the small changes within the FeCo matrix are directly related with the coercivity reduction. The tuning of these properties by simply choosing source or power open a simple path to tailor the magnetic properties.

1 Introduction

Research for soft magnetic films is always an important aspect of magnetic materials. Soft magnetic materials are extensively used in many applications such us power electronic circuits, voltage and current transformers, saturable reactors, magnetic amplifiers, inductors, and chokes. Many developments in soft magnets have been based on nanosized or nanostructured materials [1–4]. Within soft magnetic materials, $Fe_{50-70}Co_{50-30}$ are among the alloys with the highest flux densities (about 2.4T). FeCo alloys on a wide composition range are relevant due to its high saturation magnetization, low coercivity field, high permeability, and good thermal stability [5]. These physical parameters, that cannot be matched by any other alloy system, are the reason why these alloys have been widely used in the recording industry for many years and are continuously being investigated to improve their properties [6–9]. In particular, they are currently being used in the development of new spintronic devices [10,11] due to their high spin-polarized current and also in biomedicine applications like hyperthermia [12,13] where very high absorption rates have been achieved when compared to iron oxides. However, and considering soft magnetic materials applications, although they have much larger flux densities than typical permalloy films, properties like coercivity, dispersion and low anisotropy should be improved. Typical coercivities for FeCo bulk samples range from 50-100 Oe and exhibit a high positive magnetostriction [14]. Moreover, FeCo thin films can exhibit the effect of hard axis rocking consisting in a local maximum of the coercitivity along the hard axis [15]. On the other hand, properties of films synthesized by conventional sputtering techniques have proved to be strongly dependent on growing parameters like the growing power and the inert gas flux [16], pressure and substrate bias [14], underlayer materials [17], the sputtering rate [18] or the film thickness [19]. Magnetic properties of FeCo can be tailored controlling all these parameters during the fabrication process.

Pulsed DC (PDC) magnetron sputtering have been mainly used for the synthesis of thin films of isolating materials [20,21]. In this sense, it has been proved that they produce better structural quality films than DC sources used in similar conditions [22]. Pulsing the magnetron discharge makes the atoms being transported to the film having a higher energy, modifying the growth mechanism and producing smother and more dense films [23]. These small changes in morphology could have a potential large effect in the magnetic properties of soft magnetic materials, because the domain wall movement as well as magnetic anisotropy is very dependent on small structural changes. Recent works using PDC sources for tailoring magnetic properties in sputtered metallic thin films support this idea [24]. In this paper we explore the possible effects of PDC sources in the magnetic properties of CoFe thin films; comparing samples obtained using DC and PDC sputtering sources under the same growing conditions. We show that, unexpectedly, although there are no big changes in the morphology the use of different sources and growing conditions induce changes in the atomic distances within the FeCo matrix. These small changes are large enough to

† Electronic Supplementary Information (ESI) available: Scheme of the used sputtering system. See DOI: 10.1039/b000000x/

[a] *CEI Campus Moncloa, UCM-UPM, 28040 Madrid, Spain*
[b] *Dpto. de Física de Materiales, Universidad Complutense de Madrid, 28040 Madrid, Spain*
[c] *Unidad Asociada IQFR(CSIC)-UCM, Madrid 28040, Spain*
[d] *Institute for Systems based on Optoelectronics and Microtechnology (ISOM), Universidad Politécnica de Madrid, 28040 Madrid, Spain*

affect both, coercivity and direction of the easy axis, leading us to tune these properties by simple choosing power source.

2 Experimental

Samples of $Fe_{53}Co_{47}$, 20 nm thick, were grown by a DC and a Pulsed DC magnetron sputtering sources. Buffer layers of Au (5 nm) were used to promote low coercivities [18] and capping layers of Au (5 nm) were deposited to minimize the effect of oxidation. All layers were deposited sequentially without breaking vacuum at room temperature. Sputter incidence was perpendicular to the sample, so no preference anisotropy axes was induced by the effect of an oblique sputter beam. For PDC, a frequency of 155 kHz was used, with an on time of 3.55 μs and a reversed time of 2.9 μs. Si substrates (5×4 mm) were used as they have proved to be good for magnetic softness [14]. No magnetic field was applied during the growing process although it is worth to consider that the resulting magnetic fields from the magnets of the sputtering magnetron sources in the chamber on sample location was 2.6 Oe in the direction of 135^o with respect to the long sample axis, as it is depicted in the inset of Fig. 1. **An scheme of the sputtering system used is depicted in the supplementary information.**

Several complementary experimental techniques were used to characterize sample properties. Surface characterization was done by means of a Nanotec Atomic Force Microscope (AFM) operating in air. AFM images were analyzed using WSxM software [25]. The composition was determined by Oxford Instruments X-Max energy dispersive X-ray spectroscopy (EDXS). **The Auger data was measure in a ultra-high vaccum chamber with 10^{-10} mbar with a VG100AX Thermo Scientific spectrometer. Before taking the final spectra, we carefully remove the Au capping by sputtering the surface with Ar^+ ions. The sputtering were done using a differentially-pumped ion gun EX05 Vacumm Generators (working pressure 10^{-8} mbar), with 3 KeV of energy and a sputtering rate of 1 ML/min approx. Several Auger spectra were taken until no Au signal was detected in the spectra. The total sputtering time used was 20 minutes.** The crystalline structure were studied by X-ray Diffraction (XRD) using $Cu - K_\alpha$ radiation in PANalytical X-ray difractometers. X-ray absorption experiments were performed at the SpLine beamline at the European Synchrotron Radiation Facility (ESRF). We carried out X-ray absorption near edge structure (XANES) and extended X-ray absorption fine structure (EXAFS) spectroscopy experiments at the Co K-edge (7709 eV), in the range 7500-8700 eV, and in fluorescence mode. Magnetic properties have been measured in a in-built Magnetooptical Kerr effect system (MOKE). Coercivity data have been extracted from full hysteresis loops measured at room temperature with a saturating field of $\sim$ 300 Oe.

Four samples has been selected in this study, two grown with DC sputtering and two with PDC sputtering sources, and two different power values (20 W and 80 W). Depending on the growing conditions, the samples are named as DC_{20W}, DC_{80W}, PDC_{20W} and PDC_{80W}. For each growing conditions combination three samples were fabricated and analysed to confirm reproducibility in measurements.

3 Results and discussion

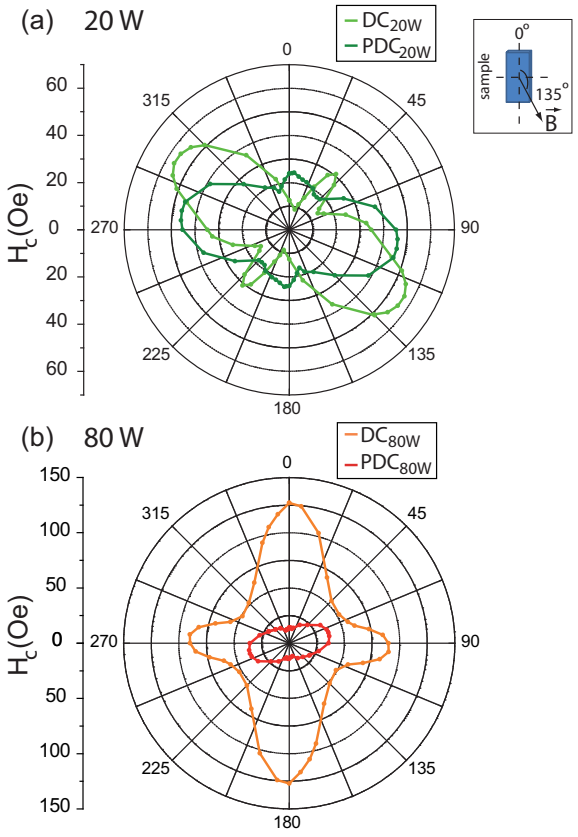

Fig. 1 Polar plots of coercivities as a function of the angle of the applied field with respect the long sample axis for (a) DC_{20W} and PDC_{20W} films, and (b) DC_{80W} and PDC_{80W} films. All samples present clear anisotropy but in the case of the samples of panel (a), the maximum value of the coercivity is less than half of samples plotted in (b). The inset shows the orientations of the applied field with respect the sample. The origin of the polar coordinates is parallel to the long samples axis.

In order to identify the origin of these changes in the magnetic properties a detailed structural analysis has been carried out. EDX spectroscopy was used to determine the composition of the CoFe layers. The samples under study

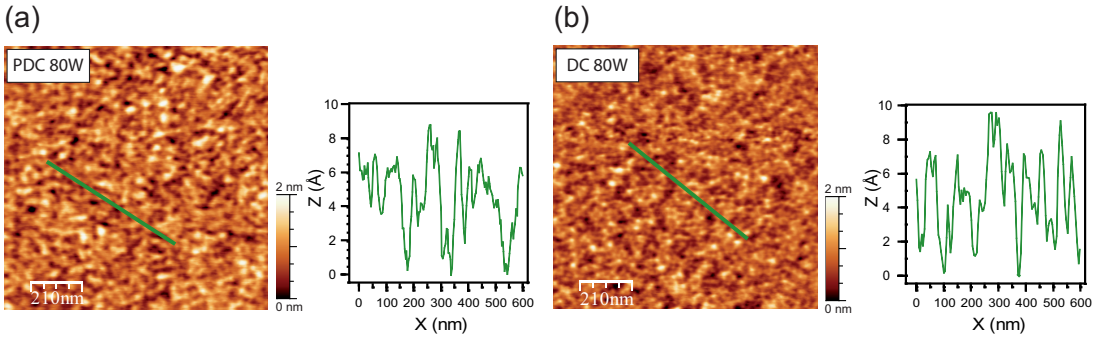

Fig. 2 AFM topological images for (a) DC 80 W and (b) PDC 80 W samples. The insets correspond to height profiles indicated in the images by the green lines. The height profiles are quite similar in both set of samples, and so do not have implications in the differences of the magnetic properties. See text for details.

are thin films (20 nm) and in these kinds of samples, the experimental error of EDXS is quite large. In order to minimize the error and increase the precision, we measured six spectra for each sample in different areas of the sample, obtaining the composition as a weighted average. The results are presented in Table 1. The analysis reveals a mean composition of $Fe_{53}Co_{47}$ in the grown thin films. From the reported data, it can be considered that all samples have the same composition within the experimental error. In fact, we have not found any change in composition above 4% in all the measured spectra. We believe that the observed differences are due to the limitation of the use of EDXS in thin films but, in any case, the differences are too small to justify the observed changes in the magnetic properties.

Table 1 EDXS mean composition of the different samples analysed in this study. The analysis reveals a mean composition of $Fe_{53}Co_{47}$ (see text for details).

Sample	Fe (weight %)	Co (weight %)
DC 20W	52.2±2.3	47.8±2.7
DC 80W	52.7±2.4	47.3±2.1
PDC 20W	55.6±2.3	44.4±2.5
PDC 20W	53.8±2.6	46.2±2.0

Surface characterization was done by means of an AFM working in tapping mode. A comparison between the profiles and topographical images for two selected DC and PDC samples are shown in Fig. 2. These samples are PDC_{80W} and DC_{80W} which correspond to those with the largest differences in magnetic properties (see Fig. 1); but the AFM images are mostly identical for all the samples we have grown, including coalescence and continuity of the films. The RMS roughness of each film was determined from measurements at more than five different randomly selected places. Image sizes were variable, from 2×2 μm^2 down to 100×100 nm^2. Results report RMS roughness of 0.23 ± 0.01 nm and 0.18 ± 0.01 nm for samples grown with DC and PDC sources respectively. The roughness of FeCo thin films appears to be mostly independent of the source used and the applied power. This small roughness is expected to have a small influence on sample coercivity, and as all samples have similar roughness, similar pinning for magnetic domain walls at the surface is expected. Therefore, the roughness cannot explain the observed magnetic differences between samples. So, neither the chemical composition nor the surface structure can justify the strong differences observed in Fig 1 regarding the magnetic properties.

X-ray diffraction patterns of all samples, measured in grazing incidence, are quite similar, showing the presence of FeCo nanocrystals and Co clusters in all samples (see Figure 3). Co peaks can be indexed as fcc-Co, a crystal phase that is probably induced by the presence of a bcc-FeCo matrix. It is established that coercivity in bcc-FeCo films is mainly related to the grain size[18]. Below the exchange length, the smaller the grain size the smaller the coercivity. Reported values for high moment FeCo exchange length are between 20-30 nm[18,26]. We have estimated the grain size from the XRD data, finding very similar data for all samples (12-14 nm for DC films and 12-20 nm for PDC films). These grain sizes cannot explain the observed magnetic behavior. In fact, the results are opposite to what it is expected, as the largest grain sizes lead to the lowest coercive fields.

The main difference found among the samples is a shift in the features of the bcc-FeCo XRD reflections. This shift could reflect the presence of internal stress in the FeCo layers. Other authors have proved that these stresses can be later reduced by thermal treatments[27]. In order to get a deeper insight, we have

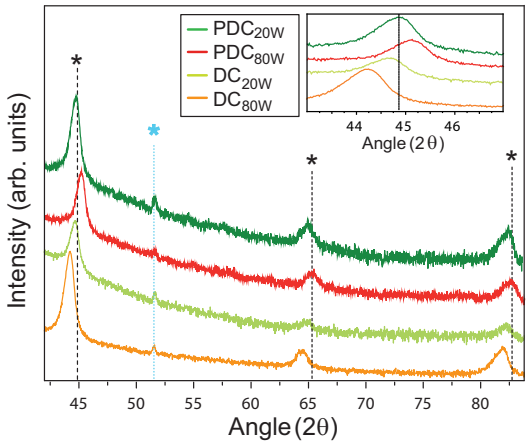

Fig. 3 X-ray diffraction diagrams of FeCo thin films samples grown with different sources (DC and PDC) and two power (20 W and 80 W). The phase reflections of the bcc-FeCo matrix are indicated with black asterisks while the blue asterisk shows the fcc phase reflections of Co. The inset enlarges the highest maximum diffraction of the bcc phase of FeCo.

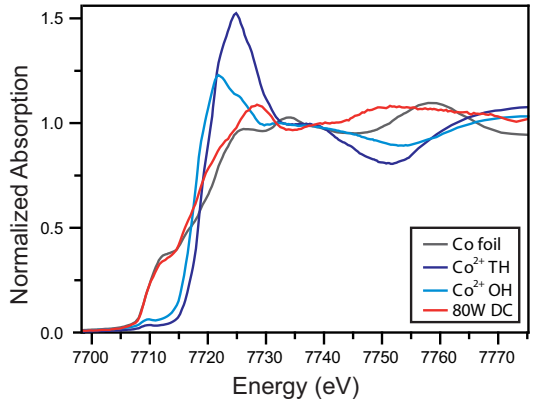

Fig. 4 Co K-edge X-ray absorption spectroscopy of FeCo DC 80 W sample. Co foil and Co^{+} in octahedral and tetrahedral positions are used as reference materials respectively. The energy position of the edge, together with the strong first peak at approximately 7720 eV of photon energy, rules out the presence of Co oxides in the films.

preformed XAS measurements. A XANES analysis shown in Fig. 4 rules out the presence of any Co oxides in the films[28]. **These results correspond to the DC_{80W} sample. We have not included results for the other samples for clarity but they have a similar shape**. The spectra of Co^{2+} ions, either in tetrahedral or octahedral positions exhibit a strong peak in the energy region between 7720 eV and 7730 eV. However, our films are depressed in this area and have a shape very similar to the Co foil both in the position of the Co K-edge and the general spectra shape. **But oxidation of Co and/or Fe could play a major role in the films magnetic behavior. To obtain the detailed chemical composition of the films we have performed Auger electron spectroscopy (AES). This analytical technique allows us to measure the chemical composition of the outermost 100 Å of a sample. An Auger spectrum from a DC_{80W} sample is depicted in Fig. 5. Although the relative intensities of the detected peaks can be slightly different depending on the sample, we have obtained the same result in all the samples analysed. As it is displayed in the inset, Fe and Co characteristic LMM Auger peaks at 600-800 eV together with the ∼50 eV Fe LMM transition are clearly observed; while no traces of oxygen is present even when the region of 500 eV is enlarged. We want to point out that the cross section for oxygen is larger than for Fe or Co, so any sign of oxidation would be clearly detected in the experimental spectrum[29]. So our Auger analysis confirms the XANES results and rules out completely the presence of any oxide, even in small-sized particles.**

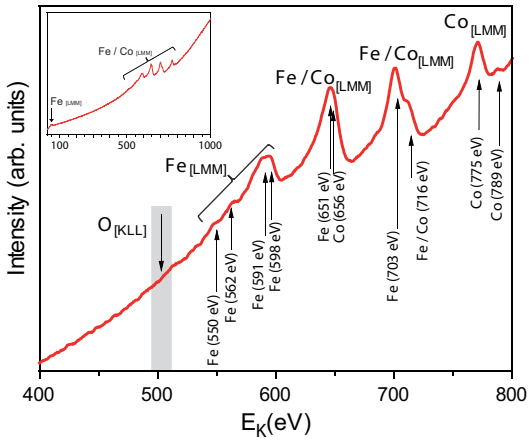

Fig. 5 Auger spectra of DC_{80W} FeCo thin film sample. No signal coming from oxygen is detected, nor in the overall spectrum (inset) neither in the area enlarged where oxygen O[KLL] transition is expected (this region, at 500 eV approx. is shaded in grey). All the samples studied in this work exhibit similar Auger spectrum shape.

The chemical analysis implies that fcc-Co or bcc-Co structures are the only one compatible with the XANES data. These structures are displayed in Fig. 6, where r_{AC} represents the distance betweens atoms A and C of the structural model.

Fig. 7 shows the Fourier Transform (FT)[30] of the Co *K*-edge spectra of the four studied samples. The overall EXAFS spectra is similar in all the cases, and both 20 W and 80 W samples exhibit features at the same radial distances. As the position of the peaks gives information about the bond lengths presented in the material, this is an indication that all samples share the same main structures. As expected, most of the fea-

tures (and the most intense ones) can be assigned to the bcc-FeCo structure. However, a simple visual inspection shows the presence of two features (the ones labeled with Greek letters) that can not be explained within a model that includes only FeCo. In order to determine the origin of these features, several structures were tested. In fact, while analyzing the fcc-Co structure, the agreement is remarkable. Whereas the first neighbour radial distance in bcc-Co ($r_{\alpha\beta}$) is hidden into the main fcc-FeCo r_{AB} peak, the second neighbour radial distance ($r_{\alpha\gamma}$) is clearly visible. The same happens with several fcc-Co distances; as their expected intensity is weak they become covered when they coincides with fcc-FeCo peaks but are clearly detected in regions without FeCo signal. This is the case for $r_{\alpha\eta}$.

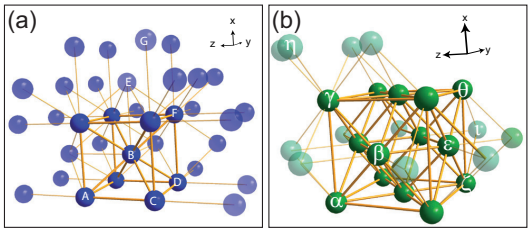

Fig. 6 Ball and stick structures of (a) bcc-FeCo and (b) fcc-Co. The labels on the atoms are used to indicate the radial distances from the corresponding central atoms(A and α respectively).

Expected and experimental radial distances obtained from EXAFS are displayed in Fig. 8, where the disparity between these two values is displayed as columns. As said before, the general agreement is remarkable, although in a closer inspection small deviations from ideal-structure distances are observed. Surprisingly, it can be noticed that no changes (less than 0.2 %) are detected in the fcc-Co cluster distances, but only in the bcc-FeCo matrix structure, being as large as ∼4% in some cases. This is an indication that the growth of Co clusters growth independently from the changes in the FeCo matrix. This is true for all the growing conditions.

The percent of deviation from ideal values indicates that the FeCo matrix is quite distorted, which most likely produces stress in the structure. We propose that the observed changes in the magnetic properties are due to the different stresses (i.e. film quality) generated during growth by changing the growing conditions. Together with the experimental dilatation/contraction of the atomic distances, Fig. 8 displays in the x-axis the coercivity of the different samples measured along the easy axis. A correlation between coercivity and deviation from the expected values of the distances is clearly observed. The best quality is achieved with the PDC source, both for 20 W and 80 W. We assign their low coercivity (46 Oe and 37 Oe respectively) to the lower deviation of the sample radial distances from the ideal ones, but also to the fact that some radial distances are even reduced, which means that along some axis the contraction of the unit cell partially compensates the dilatation in others directions. On the other hand, the most prominent changes are observed in the case of the DC_{80W} sample, which is the only sample where the distortion is always positive (and of a large value), giving rise to a dilatation of the unit cell along all the axes. So, this sample exhibits the most stressed FeCo matrix. This observation is in direct correlation with the values of the coercive field, which for this sample is more than double than in the rest of the samples (127 Oe). An intermediate result is found for the DC_{20W} sample; although the expansion is quite large for some distances (for example, +3.7% in r_{AC}), it is contracted in some others (-1.3% in r_{AB}); having its coercive field an intermediate value (56 Oe). It is important to point out that the changes in magnetic properties cannot be ascribed to exchange coupling between the FeCo layers and any antiferromagnetic oxide, as only fcc-Co is detected in the samples.

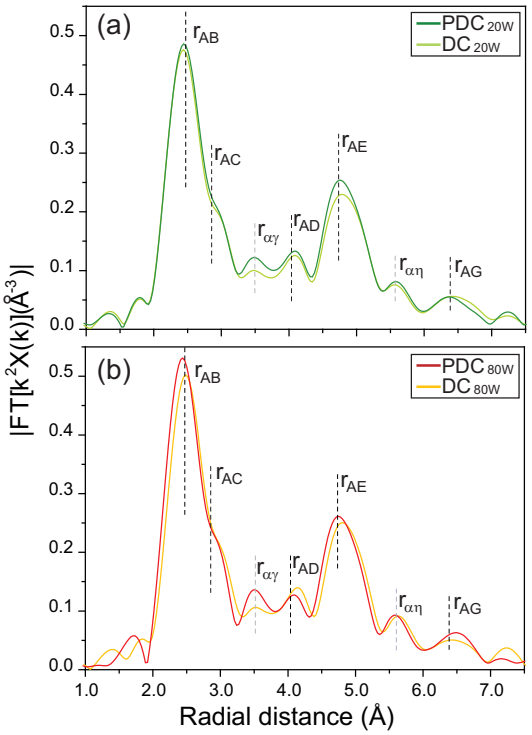

Fig. 7 Fourier transform of the Co K-edge $K^2\chi(K)$ EXAFS signals for DC and PDC magnetron sputtering for (c) 20 W and (d) 80 W. Expected radial distances of bcc-FeCo and fcc-Co are indicated with dashed line.

From Fig. 8 we can conclude that, by keeping the source, increasing the power leads to larger changes in atomic distances of the FeCo matrix. On the other hand, while keeping the same power, the PDC source produces samples with

smaller distortion and better structural quality. When the coercivity is low and the films are magnetically very soft, the magnetic field produced by the magnetron aligned the easy axis along its direction. However, when the strain increases, an additional anisotropy term forces the easy axis to align along the direction of the strain.

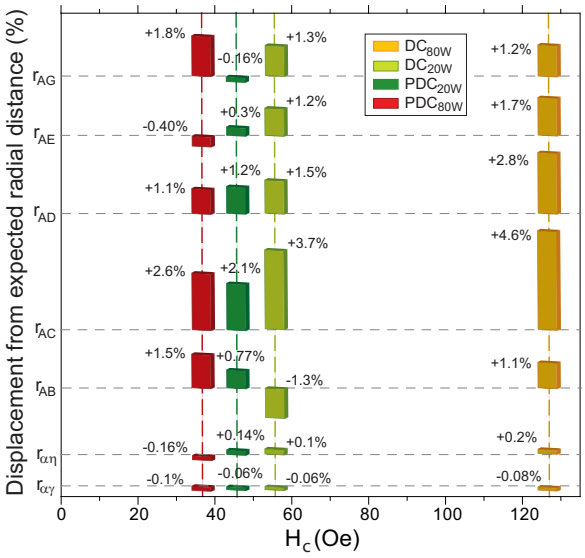

Fig. 8 Displacement from expected radial distance, expressed in percentage, for bcc-FeCo matrix and fcc-Co clusters of the four samples, obtained from EXAFS data. The values are illustrated by means of bars, which have an arbitrary thickness. The vertical dashed lines indicate the corresponding coercivity in the easy axis measured for each sample (see text for details).

4 Conclusions

We have demonstrated that, despite the utilization of the same power during the growing process, we can tune the magnetic properties of the samples depending on the source used, as the local structure strongly depends on whether the power is DC or PDC. The PDC source reduces coercivity notably in films when compared to DC films grown in similar conditions. This reduction of coercivity is not a consequence of a decrease in the **crystalline size** but seems to be associated to the **overall** better quality of the films. The bcc-FeCo matrix suffers contractions and dilatations in the structure, while keeping the fcc-Co clusters mostly unchangeable. The increase of the bcc-FeCo atomic distances is in direct correlation with the magnetic properties, as coercivity doubles when the stress is larger. On the other hand, the balance between expansion and contraction detected on PDC samples gives rise to high-quality films with very low coercivity. In addition, PDC films exhibit hard axis rocking effects and a better defined anisotropy axis. Although the relationship between stress and magnetic properties is well known, we have demonstrated that the small changes induced in the structure by changing the growth conditions are large enough to produce changes in both, coercivity and direction of the easy axis, leading us to easily tailor these properties by simple choosing source or power.

5 Acknowledgements

This work was funded by MICINN (MAT2010-21156-C03-02 and MAT2011-28751-C02-01/02). We thanks SPLINE beamline staff at the ESRF and N. Carmona and O. Rodriguez for their help during the XAS and Auger experiments respectively. Manuel Abuín acknowledges the UCM Campus of International Excellence (PICATA Program) for pre-doctoral fellowships.

References

1 D. Sellmyer and R. Skomski, *Advanced Magnetic Nanostructures*, Springer, New York, 2006.
2 Y. Yoshizawa, S. Oguma and K. Yamauchi, *J. Appl. Phys.*, 1998, **64**, 60446046.
3 K. Suzuki, A. Makino, N. Kataoka, A. Inoue and T. Masumoto, *Mater. Trans. JIM*, 1991, **32**, 93102.
4 M. A. Willard, D. E. Laughlin, M. E. McHenry, D. Thoma, K. Sickafus, J. O. Cross and V. G. Harris, *J. Appl. Phys.*, 1998, **84**, 67736777.
5 Q. F. Zhan, Z. Y. Chen, D. S. Xue and F. S. Li, *Phys. Rev. B*, 2002, **66**, 134436.
6 A. Jakobsson, E. Sasoglu, P. Mavropoulos, M. Lezaic, B. Sanyal, G. Bihlmayer and S. Blugel, *Applied Physics Letters*, 2013, **103**, 102404.
7 C. Franz, M. Czerner and C. Heiliger, *Physical Review B*, 2013, **88**, 094421.
8 V. Inturi, H. Yin, M. Kief, M. Hadley and C. Mathieu, *IEEE Transactions on Magnetics*, 2012, **48**, 1718–1722.
9 N. N. Phuoc, G. Chai and C. K. Ong, *Journal of Applied Physics*, 2012, **112**, 113908.
10 M. Bowen, V. Cros, F. Petroff, a. Fert, C. Martnez Boubeta, J. L. Costa-Kramer, J. V. Anguita, a. Cebollada, F. Briones, J. M. de Teresa, L. Morellon, M. R. Ibarra, F. Guell, F. Peiro and a. Cornet, *Applied Physics Letters*, 2001, **79**, 1655.
11 M. Romera, M. Muñoz, M. Maicas, J. Michalik, J. de Teresa, C. Magén and J. Prieto, *Physical Review B*, 2011, **84**, 1–5.
12 T. L. Kline, Y.-H. Xu, Y. Jing and J.-P. Wang, *Journal of Magnetism and Magnetic Materials*, 2009, **321**, 1525–1528.
13 H. Joisten, T. Courcier, P. Balint, P. Sabon, J. Faure-Vincent, S. Auffret and B. Dieny, *Appl. Phys. Lett.*, 2010, **97**, 253112.
14 M. Mao, T. Schneider, R. Bubber, J. Kools, X. Liu, Z. Altounian, C.-L. Lee, A. Devasahayam and K. Rook, *Journal of Applied Physics*, 2005, **97**, 10F908.
15 C. Mathieu, V. R. Inturi and M. J. Hadley, *IEEE Trans. on Mag.*, 2008, **44**, 431–434.
16 C. Mathieu, M. J. Hadley and V. R. Inturi, *Journal of Applied Physics*, 2008, **103**, 07E715.
17 X. Liu, H. Kanda and A. Morisako, *Journal of Physics: Conference Series*, 2011, **012037**, 1–6.

18 M. Vopsaroiu, M. Georgieva, P. J. Grundy, G. Vallejo Fernandez, S. Manzoor, M. J. Thwaites and K. OGrady, *Journal of Applied Physics*, 2005, **97**, 10N303.

19 T.P. Kumari, M.M. Raja, A. Kumar, S. Srinath and S.V. Kamat, *J. Magn. Magn. Mat.*, 2014, **365**, 93-99.

20 J.W. Bradley and T. Welzel, *J. Phys. D - Appl. Phys.*, 2009, **42**, 093001-23.

21 P.J. Kelly and R.D. Arnell, *Vacuum*, 2000, **56**, 159-172.

22 M. Audronis, P. Kelly, R. Arnell and a.V. Valiulis, *Surface and Coatings Technology*, 2006, **200**, 4166–4173.

23 P.J. Kelly and J.W. Bradley, *J. Optoelectron. Adv. Mater.*, 2009, **11**, 9, 1101-1107.

24 R. Ranchal, S. Fin, D. Bisero and C. Aroca, *J. Alloys and Compounds*, 2014, **582**, 839-843.

25 I. Horcas, R. Fernandez, J. M. Gomez-Rodriguez, J. Colchero, J. Gomez-Herrero and A. M. Baro, *Rev. Sci. Instrum.*, 2007, **78**, 013705.

26 X. Liu and A. Morisako, *Journal of Applied Physics*, 2008, 21–23.

27 M. D. Cooke, L.-c. Wang, R. Watts, R. Zuberek and G. Heydon, *Journal of Physics D: Applied Physics*, 2000, **1450**, 1450–1459.

28 T. Yamamoto, *X-Ray Spectrom.*, 2008, **37**, 572–584.

29 K. D. Childs, B. A. Carlson, L. A. Vanier, J. F. Moulder, D. F. Paul, W. F. Stickle, and D. G. Watson,*Handbook of Auger Electron Spectroscopy*, 1995, C. L. Hedberg, Ed..

30 E. Sayers and B. A. Bunker, *X-Ray Absorption: principles, Aplications and Techniques of EXAFS, SEXAFS and XANES*, Willey, New York, 1988.

Changes of coercitivity and EXAFS atomic distances obtained for 20 nm $Fe_{65}Co_{35}$ thin films grown with DC and PCD magnetron sputtering.